The lattice position of Fe in Fe-doped $LiNbO_3$

1995 J. Phys.: Condens. Matter 7 6971

(http://iopscience.iop.org/0953-8984/7/35/004)

J. Phys.: Condens. Matter 7 (1995) 6971–6980. Printed in the UK

The lattice position of Fe in Fe-doped $LiNbO_3$

Th Gog†, P Schotters†, J Falta†, G Materlik† and M Grodzicki‡

† Hamburger Synchrotronstrahlungslabor HASYLAB am Deutschen Elektronen-Synchrotron DESY, 22603 Hamburg, Germany

‡ Institut für Physik, Medizinische Universität, 23538 Lübeck, Germany

Received 7 February 1995

Abstract. The lattice location of Fe atoms in Fe-doped $LiNbO_3$ is determined experimentally employing x-ray standing waves. At a bulk concentration of 7.48×10^{18} cm^{-3} Fe is found to occupy sites close to the ferroelectric Li position, shifted by 0.18 Å in the direction of the $-c$ axis. Electronic structure calculations confirm this result insofar as computed spectroscopic data are more consistent with the respective experimental values for Fe located in the vicinity of the Li site than for Fe occupying the Nb lattice position.

1. Introduction

Among the numerous technical applications of ferroelectric lithium niobate ($LiNbO_3$) is the holographic storage of information in this versatile material, mediated by what is known as the photorefractive effect (Buse *et al* 1994). This effect is assumed to proceed in two stages. First, an incident light field generates electric currents via bulk photovoltaic processes leading to non-uniform space charge distributions. Second, the associated electric fields in turn modulate the refractive index of this material via the electrooptic effect. The disturbed state of refractive index can be fixed by certain means and used to recreate the original light field at a later time effectively providing storage of a volume phase hologram.

The photorefractive effect in $LiNbO_3$ can drastically be enhanced by doping with transition metals, Fe and Cu being the most widely used ones. While the leading role of these dopants in this context as well as the dominance of photovoltaic currents over diffusion and drift processes has been studied extensively (Kurz *et al* 1977), a detailed description of microscopic mechanisms steering the photorefractive effect is still pending. As an approach towards a solution of this problem the lattice position of Fe atoms in $LiNbO_3$ has been studied both experimentally with x-ray standing waves, and theoretically by cluster calculations in the local density approximation.

2. X-ray standing waves

The term 'x-ray standing waves (XSW)' refers to an experimental technique which was developed as an offspring of the dynamical theory of x-ray diffraction and fuelled by the advent of high-intensity synchrotron radiation sources. It is particularly well suited to determine lattice locations of dilute impurity atoms at the surface or in the bulk of nearly perfect crystals.

When a plane wave of x-rays is diffracted by a set of (*hkl*) diffraction planes in a perfect crystal, incident and diffracted beams interfere to form a standing wave field which

0953-8984/95/356971+10$19.50

has the periodicity of the lattice planes and shifts into the crystal by an amount of half a planar spacing as the incident angle is advanced towards higher angles through the Bragg reflection. Secondary yields such as fluorescence from impurity atoms will be modulated accordingly and, comparing the phase of the measured signal with the known phase of the standing wave field with regard to the diffraction planes, the relative position of the impurity within a planar spacing is immediately revealed.

In an actual XSW measurement normalized fluorescence yields Y_H are fitted to an expression derived from dynamical diffraction theory,

$$Y_H(\theta) = Z(\theta)\left\{1 + R_H(\theta) + 2P\sqrt{R_H(\theta)}f_c^H \cos(\nu_H(\theta) - 2\pi\Phi_c^H)\right\}$$

where R_H denotes the reflectivity, P is a polarization constant and ν_H is the standing wave phase relative to the diffraction planes associated with H. $Z(\theta)$ is the normalized effective thickness contributing to the yield. It is determined by the attenuation of the wave field inside the crystal and the reabsorption of the fluorescence signal including contributions from both linear absorption and primary extinction. Two parameters, namely the coherent position Φ_c^H and the coherent fraction f_c^H are extracted from the fits, determining phase and magnitude of the (hkl) Fourier component of the impurity atom distribution. In the case where this distribution is determined by a single atomic site, Φ_c^H is the relative position of this site within a planar spacing and f_c^H is the percentage of atoms occupying this site. A more detailed description of this method including experimental considerations can be found in the articles by Hertel *et al* (1985) and Bedzyk and Materlik (1986). In the present case a complete three-dimensional determination of the Fe position is based on four reflections, namely $(0, 1, \bar{4})$, $(1, \bar{1}, \bar{4})$, $(\bar{1}, 0, \bar{4})$ and $(0, 0, \bar{6})$. For the latter two XSW measurements were conducted, while the coherent position and the coherent fraction for the first two were deduced from symmetry arguments. This set of reflections is particularly well suited for the task at hand since both the Nb and Li atoms as well as the 'structural vacancy' form single atomic sheets with respect to the corresponding diffraction planes.

3. Experimental results

Congruently grown z-cut wafers of $LiNbO_3$, produced commercially by Crystal Technology, served as samples in this investigation. Doped in the melt with 0.015 wt.% Fe the effective, homogeneous bulk concentration of dopants in these wafers was 7.48×10^{18} cm^{-3}.

The XSW experiments were performed at the RÖMO I station of the Hamburger Synchrotronstrahlungslabor HASYLAB. XSW data for the normalized reflectivity and Nb and Fe fluorescence along with theoretical, fitted curves are shown in figures 1 and 2 for the $(1, \bar{1}, \bar{4})$ and $(0, 0, \bar{6})$ reflections respectively. A summary of coherent positions and coherent fractions extracted from these fits is given in table 1.

Table 1. Coherent positions and coherent fractions extracted from the XSW measurements. Coherent positions Φ are given in units of diffraction plane spacing $d_{(1,\bar{1},\bar{4})} = 2.74$ Å and $d_{(0,0,\bar{6})} = 2.31$ Å respectively, with $(\Phi = 0)$ being located on planes containing Nb atoms.

Reflection	Φ_{Fe}	f_{Fe}	Φ_{Nb}	f_{Nb}
$(1, \bar{1}, \bar{4})$	0.92 ± 0.02	0.67 ± 0.02	1.00 ± 0.04	0.98 ± 0.03
$(0, 0, \bar{6})$	0.38 ± 0.04	0.49 ± 0.03	1.00 ± 0.04	0.97 ± 0.03

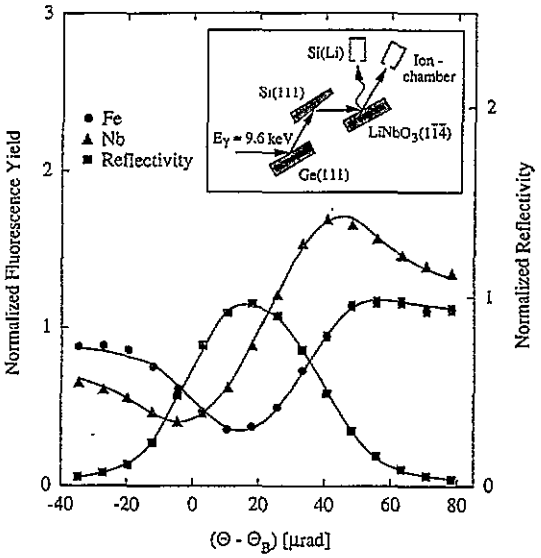

Figure 1. Normalized XSW data and corresponding theoretical curves as a function of angle for the $LiNbO_3(1, \bar{1}, \bar{4})$ reflection. Coherent positions in units of the diffraction plane spacing and coherent fractions for Nb and Fe atoms emerge as $\Phi_{Fe} = (0.92 \pm 0.02)$, $f_{Fe} = (0.67 \pm 0.02)$, $\Phi_{Nb} = (1.00 \pm 0.04)$, $f_{Nb} = (0.98 \pm 0.03)$. The experimental set-up and the combination of monochromator and sample crystals are shown in the inset.

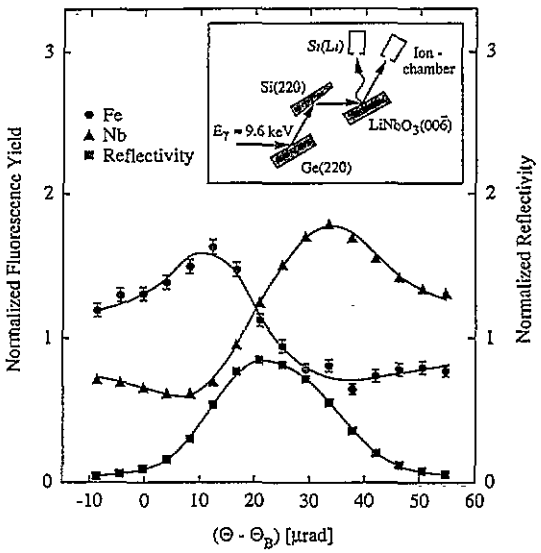

Figure 2. Normalized XSW data and corresponding theoretical curves as a function of angle for the $LiNbO_3(0, 0, \bar{6})$ reflection. Coherent positions in units of the diffraction plane spacing and coherent fractions for Nb and Fe atoms emerge as $\Phi_{Fe} = (0.38 \pm 0.04)$, $f_{Fe} = (0.49 \pm 0.03)$, $\Phi_{Nb} = (1.00 \pm 0.04)$, $f_{Nb} = (0.97 \pm 0.03)$. The experimental set-up and the combination of monochromator and sample crystals are shown in the inset.

Considering single-site occupancy for Fe atoms and an undistorted $LiNbO_3$ host lattice as shown in figure 3, the XSW results are easily interpreted. From the conservation of the

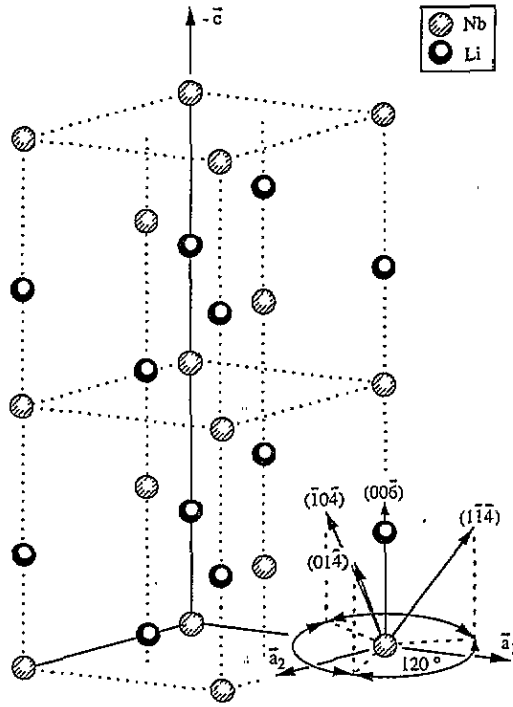

Figure 3. The hexagonal unit cell of the $LiNbO_3$ structure; oxygen atoms are omitted for clarity. Directions of the four scattering vectors associated with reflections utilized in the present XSW study are indicated.

threefold rotational symmetry of the c axis, which was shown in a similar XSW study on Ti:$LiNbO_3$ (Gog *et al* 1994), it follows that the three equivalent reflections $(0, 1, \bar{4})$, $(1, \bar{1}, \bar{4})$, $(\bar{1}, 0, \bar{4})$ have to yield identical coherent positions leading to a restriction of possible Fe sites to stacks formed by Nb and Li atoms parallel to the c axis. Furthermore the measured position of $\Phi_{Fe,(1,\bar{1},\bar{4})} = (0.92 \pm 0.02)$ places Fe either in the close vicinity of the Li site ('1' in figure 4) or near the Nb site ('2' in figure 4) on these stacks, the ambiguity between site 1 and 2 arising from the fact that two structurally different parts of the unit cell are enclosed alternately between $(1, \bar{1}, \bar{4})$ diffraction planes. This ambiguity is resolved by including the coherent position from the $(0, 0, \bar{6})$ measurement $\Phi_{Fe,(0,0,\bar{6})} = (0.38 \pm 0.03)$, which selects site 1 as the valid Fe position while excluding site 2. Measured coherent positions for Nb atoms of $\Phi_{Nb,(1,\bar{1},\bar{4})} = (1.00 \pm 0.04)$ and $\Phi_{Nb,(0,0,\bar{6})} = (1.00 \pm 0.04)$ indicate that from the viewpoint of the standing wave field the host structure is indeed undistorted. Reexamining the results it is noted, however, that the coherent fraction for Fe atoms is significantly higher in the measurement using the oblique $(1, \bar{1}, \bar{4})$ reflection than in the measurement using $(0, 0, \bar{6})$. This effect has been observed also in other samples doped with Ti and Er (Gog *et al* 1994, 1993). It strongly suggests that these dopants do not occupy just a single site but obey a distribution function which is extended in the c direction so that its smaller projection upon the $(1, \bar{1}, \bar{4})$ direction leads to a higher value of f_c in this direction. Gaussian distributions have been considered and it was found that a maximal FWHM of 1.06 Å is still consistent with the data.

Summarizing the XSW measurements, the lattice position for an assumed single-site

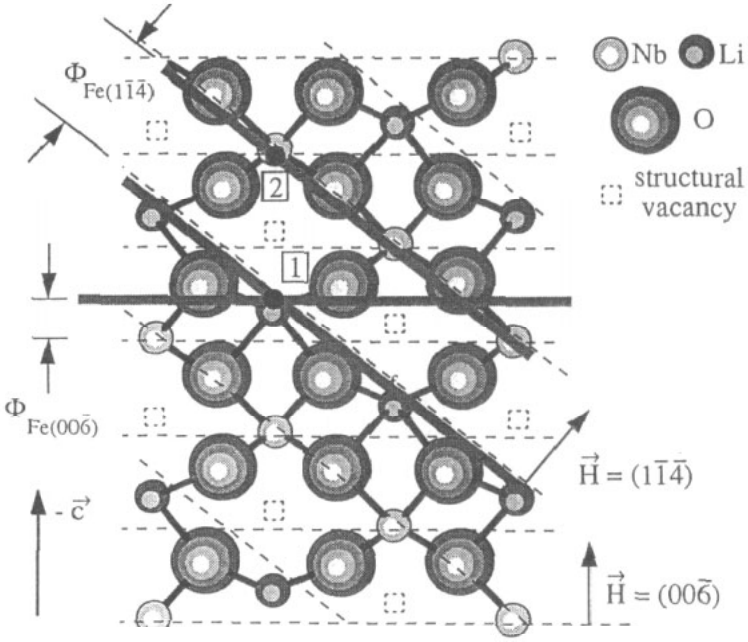

Figure 4. A diagonal cut through the hexagonal unit cell. Darkly shaded bars mark the measured coherent position of Fe atoms with respect to the $(1, \bar{1}, \bar{4})$ and $(0, 0, \bar{6})$ planes. The widths of these bars correspond to the experimental error. Positions 1 and 2 emerge as possible Fe sites when only the result of the $(1, \bar{1}, \bar{4})$ measurement together with the threefold symmetry of the c axis is considered. Including the $(0, 0, \bar{6})$ measurement leaves site 1 as the only valid Fe position.

occupancy of Fe atoms in the $LiNbO_3$ structure is determined to be (0.18 ± 0.07) Å above the ferroelectric Li site in the $-c$ direction. However, due to the systematic difference in coherent fractions for the $(0, 0, \bar{6})$ and $(1, \bar{1}, \bar{4})$ measurements, a spread of positions in a range of up to ± 0.7 Å is conceivable. This conclusion is consistent with earlier assertions from a PIXE/channelling study (Rebouta *et al* 1991) and an EXAFS study (Prieto and Zaldo 1992).

4. Theoretical studies

In a first step, electronic structure calculations have been performed on Fe-free $LiNbO_3$ clusters. In the second step various possible sites for Fe within these clusters were investigated by computing some spectroscopic data for which experimental values are available. All calculations have been carried out within the local density approximation (LDA) by the spin-polarized self-consistent charge X_α (SCC X_α) method (Grodzicki 1980, 1985, Bläs *et al* 1987).

The $LiNbO_3$ clusters have been constructed in such a way that they fulfil the following conditions:

(i) the six oxygen atoms nearest to the lithium atom to be substituted by Fe have their full crystalline environment consisting of four cations;

(ii) the two neighbouring Nb atoms on the c axis are included with their oxygen

octahedra;

(iii) all oxygen atoms are surrounded by at least three cations in order to remove the effects of dangling bonds of oxygen on the band gap and to produce a sufficiently stabilizing electrostatic potential;

(iv) the total charge of the cluster should be as close to zero as possible which requires substitution of all terminating Nb atoms by Li, denoted as Li_t;

(v) the threefold symmetry with regard to the c axis has to be preserved.

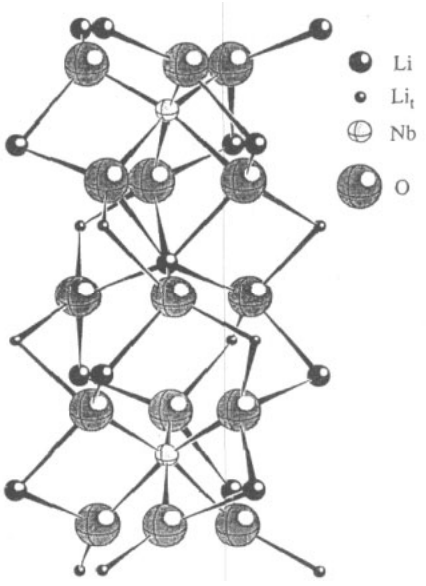

Figure 5. The smallest cluster, containing 39 atoms altogether, which was used in the electronic structure calculations. To minimize the total charge, all terminating Nb atoms were substituted by Li atoms, denoted by Li_t and displayed as small black spheres in the figure.

The smallest clusters fulfilling these conditions contain 39, 67 and 82 atoms, respectively. The 39-atom cluster is shown in figure 5. The atomic orbital basis consists of 2s, 2p orbitals at O, 2s orbitals at Li, Li_t and 5s, 4d orbitals at Nb. The resulting characteristic data of the three clusters (number of atoms, electrons and basis orbitals) are displayed in table 2, together with the total charges and the calculated band gap. It is seen that all clusters carry a positive charge, mainly due to condition (ii) above. Achieving charge neutrality would require the removal of some of the terminating cations which in turn, however, yields an almost vanishing band gap due to unsaturated oxygen 2p orbitals and reduction of the stabilizing electrostatic potential of the cations. Hence, for all three clusters the calculated band gaps are still considerably smaller than the measured band gap of bulk $LiNbO_3$ of 3.7 eV because the states at the top of the valence band arise from the 2p orbitals of the oxygen atoms with only threefold cationic coordination. The charge distribution of the three clusters is shown in table 3. Whereas the average effective charge of oxygen remains virtually unchanged, the effective charge of Nb increases steadily accompanied by a reduction of the overlap population of the Nb–O bond, i.e. the Nb–O bond becomes more ionic with increasing cluster size even though a value of 2.48 still indicates a strong covalent bond, unlike the Li–O bond, showing much more ionic character. This result is in qualitative agreement with conclusions from NMR measurements (Peterson *et al* 1968);

assuming a charge of +1 for Li, values for the charge of O and Nb are deduced as −0.86 and +1.59, respectively.

Table 2. Characteristic data of model clusters.

Atoms								
Total	Nb	O	Li	Li_t	Electrons	Orbitals	Cluster charge	Band gap (eV)
39	2	15	13	9	120	94	+2	1.23
67	5	27	23	12	216	173	+6	1.57
82	8	36	26	12	288	230	+6	1.97

Table 3. Average effective charges Q and overlap populations n(A,B) for $LiNbO_3$ model clusters.

No of atoms	Q(Nb)	Q(O)	Q(Li)	n(Nb,O)	n(Li,O)
39	0.92	−0.84	0.59	2.99	0.72
67	1.26	−0.90	0.69	2.65	0.41
82	1.45	−0.88	0.69	2.48	0.41

Turning next to the Fe-doped $LiNbO_3$, calculations have been performed for Fe replacing Li as well as Nb. Placing Fe at the structural vacancy site without removing any cation yielded unreasonable results because the short Fe–Nb distance of 1.96 Å leads to strong electrostatic repulsive interactions between the cations. Therefore, such a position seems to be unlikely without admitting large distortions of the host lattice and has been excluded.

Starting with the position derived from XSW measurements, the respective one-electron energies of Fe in the formal oxidation state II, Fe(II), in the 82-atom cluster are shown in figure 6 for three different spin states. The splitting of the Fe(3d) orbitals represents a pattern typical for a trigonally distorted octahedron with a higher-lying twofold degenerate level (symmetry e or e_g in octahedral symmetry) and three lower-lying levels (symmetry a_1, e or t_{2g} in octahedral symmetry) exhibiting a small splitting due to the distortion. The calculated orbital energy difference corresponding approximately to the crystal field splitting varies for the high-spin state between 0.67 eV for Fe(II) in the 82-atom cluster (figure 6) and 1.22 eV for Fe(III) in the 39-atom cluster. These results are in reasonable agreement with the experimental value of 1.1 eV derived from optical absorption spectroscopy (Kurz *et al* 1977). Comparing the total energies of Fe(II) for different spin states (figure 6), the high-spin state turns out to be the ground state in accordance with conclusions derived from Mössbauer spectroscopy (Keune *et al* 1975, 1976).

The crystal field splitting of the 3d orbitals for Fe at the Nb position was calculated with a result between 1.85 eV and 2.01 eV for all spins and both oxidation states of Fe. The computed ground state of Fe(III) is the low-spin ($S = \frac{1}{2}$) configuration, whereas for Fe(II) it is the intermediate-spin state ($S = 1$) which has the lowest energy. Both results are in contradiction to the Mössbauer experiments, even though local spin density calculations usually favour high-spin states. Thus, the large crystal field splitting as well as the wrong spin state provide compelling evidence against Fe at the Nb position if larger distortions of the host lattice are excluded.

Finally, the calculated charge distribution around the Fe site has been used to compute the quadrupole splitting. Experimentally, this has been determined by Mössbauer

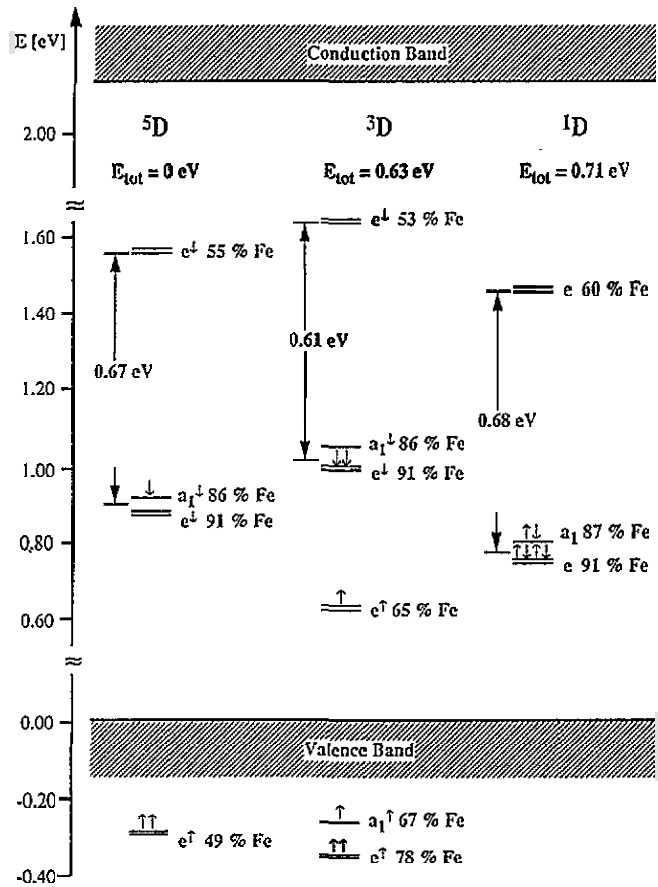

Figure 6. One-electron energies of Fe(II) at the experimental position for the 82-atom cluster. Total energies are given relative to the high-spin state. For clarity, the energy difference between a_1 and e states of about 4 meV is not drawn to scale.

spectroscopy (Keune *et al* 1975, 1976), revealing Fe to occur in both oxidation states, Fe(II) and Fe(III). The measured quadrupole splitting of Fe(III) is virtually independent of temperature with a value of $+0.53$ mm s^{-1}, whereas for Fe(II) a pronounced temperature dependence has been observed, ranging from -2.46 mm s^{-1} at 4.2 K to -1.73 mm s^{-1} at 295 K. The quadrupole splitting ΔE_Q is related to the main component V_{zz} of the electric field gradient (efg) tensor by

$$\Delta E_Q = \tfrac{1}{2} e^2 Q V_{zz} (1 + \eta^2/3)^{1/2}.$$

In the calculations, the nuclear quadrupole moment Q of ^{57}Fe is taken to be 0.15 barn (Bominaar *et al* 1989), and the asymmetry parameter $\eta = |V_{xx} - V_{yy}|/|V_{zz}|$ vanishes due to assumed threefold asymmetry of the Fe position. The components V_{ij} of the efg tensor have been calculated as described earlier (Grodzicki *et al* 1987). Since the efg can be rather sensitive to variations in geometry, the position of Fe has been varied along the c axis, starting from the ferroelectric position of Li ($\Delta c = 0$ Å), passing through the experimentally determined value down to $\Delta c = -0.4$ Å, thus approaching the position of Li in the paraelectric phase ($\Delta c = -0.46$ Å). For comparison, the vertical distance between two neighbouring Nb atoms is 6.93 Å.

Table 4. Calculated and experimental quadrupole splittings ΔE_Q (mm s^{-1}) for Fe(II) and Fe(III) as function of cluster orbital occupation $n(a_1)$, $n(e)$ and position Δc (Å) with respect to the ferroelectric Li site.

		Δc (Å)					Experimental
	$n(a_1)/n(e)$	0.0	−0.1	−0.2	−0.3	−0.4	(Keune *et al* 1975)
Fe(II)[a]	1.0/0.0	−3.29	−3.17	−3.05	−2.94	−2.85	from
	0.8/0.2	−2.39	−2.38	−2.37	−2.37	−2.36	−2.46 (4.2 K)
	0.6/0.4	−1.49	−1.59	−1.70	−1.81	−1.89	to
	0.4/0.6	−0.16	−0.80	−1.03	−1.24	−1.41	−1.73 (295 K)
	0.2/0.8	+0.29	−0.02	−0.36	−0.68	−0.94	
	0.0/1.0	+1.18	+0.77	+0.31	−0.12	−0.46	
Fe(III)	0.0/0.0	−0.02	+0.01	+0.08	+0.18	+0.34	+0.53

[a] Neglecting spin–orbit coupling.

The calculated ΔE_Q for Fe(III) increases slightly in going from $\Delta c = 0$ Å to $\Delta c = -0.4$ Å, but is always smaller than the experimental value (last row of table 4). This may be interpreted as an indication for a slight additional distortion of the surrounding oxygen atoms which may even remove the threefold symmetry resulting in a nonvanishing asymmetry parameter (Engelmann *et al* 1987).

Such a distortion may also affect the splitting of the a_1 and e levels within the t_{2g} manifold which is essential for size, sign and temperature dependence of the quadrupole splitting of Fe(II). Apart from such a possible distortion, the splitting and ordering of the a_1 and e levels cannot be determined conclusively by the cluster calculations for the following reasons. First, it varies from cluster to cluster: in the 39-atom cluster a_1 is lower by 0.1 eV than e, whereas in the 67-atom and the 82-atom clusters a_1 is higher than e by 3 meV and 4 meV, respectively. Second, the correct splitting of a_1 and e for Fe(II) can be determined quantitatively only after including spin–orbit coupling which has not been done in the current calculations. However, the experimental Mössbauer spectra of Fe(II) clearly indicate that a_1 must be below the e level since a reversed order leads to considerably different results (Paulsen *et al* 1994). Additionally, the strong temperature dependence of ΔE_Q allows the conclusion that the splitting is small enough for the e level to become populated appreciably at room temperature. Therefore, the quadrupole splitting of Fe(II) has been computed as a function of the relative occupancy of the a_1 and e spin down cluster orbitals. Despite the various theoretical approximations and the uncertainty in the Fe position, the results in table 4 strongly suggest that at low temperatures the ground state configuration is mainly $^5A_1$ with an admixture of the ^5E configuration of less then 20%, taking into account that spin–orbit coupling generally reduces $|\Delta E_Q|$. In addition, the temperature dependence of ΔE_Q can be simulated by thermal population of the e orbital, and the observed reduction by 0.73 mm s^{-1} (Keune *et al* 1975) is well reproduced if an energy difference of about 30 meV between a_1 and e is assumed.

In summing up, the theoretical results are most consistent with available experimental data (crystal field splitting, spin state, quadrupole splitting) if Fe in both oxidation state is placed between the Li positions in the ferroelectric and paraelectric phase. Reproducing the correct spin state and crystal field splitting for Fe at the Nb position would require substantial distortion of the host lattice which may be energetically unfavourable.

5. Conclusions

On the basis of the XSW measurements performed, the lattice position of Fe in $LiNbO_3$ has been determined to be a position shifted from the ferroelectric Li site by 0.18 ± 0.07 Å in a direction towards the paraelectric Li site. However, due to systematic differences in the coherent fraction of the measurements a narrow spread of positions is also consistent with the data.

Electronic structure calculations employing the experimental result of Fe being located near the ferroelectric Li position yields values for crystal field splitting, spin state and quadrupole splitting that are considerably more consistent with the respective spectroscopic data than calculations based on Fe located at the Nb site.

Thus, both experimental and theoretical evidence contradicts the longstanding assertion that Fe should occupy the Nb lattice position for reasons of charge balance. Nevertheless, due to the inherent defect structure of congruent $LiNbO_3$, the process of incorporation can be interpreted by Fe replacing Nb atoms in antisite defects located at the Li site.

Acknowledgment

The authors acknowledge valuable discussions with A X Trautwein.

References

Bedzyk M J and Materlik G 1986 *Phys. Rev.* B **32** 6456
Bläs R, Guillin J, Bominaar E L, Grodzicki M, Marathe V R and Trautwein A X 1987 *J. Phys. B: At. Mol. Phys.* **20** 5627
Bominaar E L, Guillin J, Sawaryn A and Trautwein A X 1989 *Phys. Rev.* B **39** 72
Buse K, Jermann F and Krätzig E 1994 *Appl. Phys.* A **58** 191
Engelmann H, Gatzweiler W, Gonser U, Dezsi I and Balogh A G 1987 *J. Non-Cryst. Solids* **89** 326
Gog Th, Griebenow M and Materlik G 1993 *Phys. Lett.* **181A** 417
Gog Th, Harasimowicz T, Dev B N and Materlik G 1994 *Europhys. Lett.* **25** 253
Grodzicki M 1980 *J. Phys. B: At. Mol. Phys.* **13** 2683
——1985 *Thesis of Habilitation* Hamburg
Grodzicki M, Männing V, Trautwein A X and Friedt J M 1987 *J. Phys. B: At. Mol. Phys.* **20** 5595
Hertel N, Materlik G and Zegenhagen J 1985 *Z. Phys.* B **58** 199
Keune W, Date S K, Dezsi I and Gonser U 1975 *J. Appl. Phys.* **46** 3914
Keune W, Date S K, Gonser U and Bunzel H 1976 *Ferroelectrics* **13** 443
Kurz H, Krätzig E, Keune W, Engelmann H, Gonser U, Dischler B and Räuber A 1977 *Appl. Phys.* **12** 355
Paulsen H, Ding X Q, Grodzicki M, Butzlaff Ch, Trautwein A X, Hartung R and Wieghardt K 1994 *Chem. Phys.* **184** 149
Peterson G E and Bridenbaugh P M 1968 *J. Chem. Phys.* 48 3402
Prieto C and Zaldo C 1992 *Solid State Commun.* **83** 819
Rebouta L, Da Silva M F, Soares J C, Hage-Ali M, Stoquert J P, Siffert P, Sanz-Garcia J A, Diéguez E and Agulló-López F 1991 *Europhys. Lett.* **14** 557